Applied Catalysis B: Environmental 259 (2019) 118127

Contents lists available at ScienceDirect

Applied Catalysis B: Environmental

journal homepage: www.elsevier.com/locate/apcatb

On the positive effect of UVC light during the removal of benzothiazoles by photoelectro-Fenton with UVA light

Anlin Xu[a,b], Enric Brillas[a], Weiqing Han[b], Lianjun Wang[b], Ignasi Sirés[a,*]

[a] Laboratori d'Electroquímica dels Materials i del Medi Ambient, Departament de Química Física, Facultat de Química, Universitat de Barcelona, Martí i Franquès 1-11, 08028, Barcelona, Spain

[b] Key Laboratory of Jiangsu Province for Chemical Pollution Control and Resources Reuse, School of Environmental and Biological Engineering, Nanjing University of Science and Technology, Nanjing, 210094, China

ARTICLE INFO

Keywords:
2-Hydroxybenzothiazole
Benzothiazole
Gas-diffusion electrode
Photoelectro-Fenton process
Water treatment

ABSTRACT

Benzothiazole (BTH) and 2-hydroxybenzothiazole (2-OH-BTH) are ubiquitous pollutants in aquatic ecosystems. This article reports their photoelectro-Fenton (PEF) treatment, either alone or mixed, in sulfate medium at pH 3.0 using an IrO_2-based/air diffusion cell that generates H_2O_2 under UVA and/or UVC irradiation. UVC-PEF was more effective than UVA-PEF to remove the target pollutants, which suggests a positive impact of $^{\cdot}OH$ formed via Fenton's reaction and photo-induced homolysis of H_2O_2 in the former method. In addition, BTH disappeared more quickly than 2-OH BTH. Full-time UVA-/UVC-PEF outperformed UVC-PEF and UVA-PEF to mineralize the mixtures, although requiring a much higher energy consumption. The evolution of generated H_2O_2 and homogeneous $^{\cdot}OH$ confirmed the positive contribution of UVC photolysis in UVA-PEF. Part-time use of UVC radiation in UVA-PEF yielded a similar total organic carbon removal, with much lower energy consumption. BTH was oxidized to 2-OH-BTH, which was subsequently transformed into other five heteroaromatics.

1. Introduction

In recent years, hydrogen peroxide has become a key large-scale green commodity [1]. Among its multiple uses, H_2O_2-based advanced oxidation processes (AOPs) have acquired an extraordinary relevance for the removal of organic contaminants from water [2]. In particular, its catalytic decomposition promoted by Fenton's Reaction (1) enhances very significantly the oxidation power of H_2O_2, since it is quickly converted to homogeneous hydroxyl radical ($^{\cdot}OH$) with much greater standard redox potential (E^{o} = 2.80 V/SCE at pH = 0) [3,4].

$$Fe^{2+} + H_2O_2 \rightarrow Fe^{3+} + {}^{\cdot}OH + OH^{-} \quad (1)$$

Electro-Fenton (EF) process can be considered a more sustainable approach as compared to conventional Fenton process. The electrochemical production of H_2O_2 on demand from Reaction (2) [5–7] in EF counteracts several inherent drawbacks of H_2O_2 as a chemical reagent, including its high cost.

$$O_{2(g)} + 2H^{+} + 2e^{-} \rightarrow H_2O_2 \quad (2)$$

Highly electrocatalytic materials for Reaction (2) include carbon-based ones like carbon nanotubes [8,9], reticulated vitreous carbon [10], carbon or graphite felt [10–14] and carbon-polytetrafluoroethylene (PTFE) composites [6,13,15–17].

Nonetheless, EF still presents a crucial limitation, which is the partial or at least very slow degradation of some refractory intermediates generated during the treatment like the Fe(III)-carboxylate complexes [3]. This can be overcome by means of the photoelectro-Fenton (PEF) process, which has originated the most effective series of systems among the so-called electrochemical advanced oxidation processes (EAOPs) [18]. In the most typical UVA-PEF, UVA photons (λ = 315–400 nm) catalyze the photolysis of all Fe(III) species, including [18–24]: (i) the photoreduction of its aqueous complexes according to photo-Fenton Reaction (3), which acts in concomitance with cathodic Fe(III) electroreduction to preserve the catalytic Fe(III)/Fe(II) cycle, eventually increasing the number of oxidants, and (ii) the photodecomposition of Fe(III)-carboxylate complexes from Reaction (4).

$$[Fe(OH)]^{2+} + h\nu \rightarrow Fe^{2+} + {}^{\cdot}OH \quad (3)$$

$$[Fe(OOCR)]^{2+} + h\nu \rightarrow Fe^{2+} + CO_2 + R^{\cdot} \quad (4)$$

Some authors have explored the use of UVC-PEF [25–28] and even vacuum-UV-PEF [28], where photons with λ < 290 nm cause the homolysis of H_2O_2, as shown in Reaction (5). Furthermore, UVC light can contribute to direct photolysis of aromatic molecules. However, in

* Corresponding author.
E-mail address: i.sires@ub.edu (I. Sirés).

https://doi.org/10.1016/j.apcatb.2019.118127
Received 19 April 2019; Received in revised form 26 July 2019; Accepted 24 August 2019
Available online 25 August 2019

UVC-PEF, the role of Fenton's Reaction (1) becomes much less significant due to the preponderance of Reaction (5) to form $^{\cdot}OH$ [26,27]. UVC-PEF is thus similar to H_2O_2/UVC process, being less effective and more expensive than UVA-PEF. Lately, UVA-PEF has evolved towards solar PEF (SPEF) process, which has achieved the greatest efficiencies among all EAOPs due to the high power output of natural sunlight [29–33].

$$H_2O_2 + h\nu \rightarrow 2^{\cdot}OH \quad (5)$$

Despite the superiority of SPEF, UV lamps are still needed to operate either in regions with low solar irradiation or in continuous water treatment units. In UVA-PEF, the gas-diffusion electrode (GDE) is the preferred cathode material [19,20,23,24], because it allows attaining a high H_2O_2 mass production rate [33]. However, since only a catalytic Fe^{2+} amount is employed, an excess of H_2O_2 tends to be accumulated, which is detrimental because it acts as a radical scavenger according to parasitic Reaction (6). A potential solution could then be to implement a dual UVA-/UVC-PEF process, where the excess of H_2O_2 is destroyed by UVC photons, thus producing additional amounts of $^{\cdot}OH$ from Reaction (5). Worth highlighting, such combination has never been explored so far.

$$H_2O_2 + {}^{\cdot}OH \rightarrow H_2O + HO_2^{\cdot} \quad (6)$$

In an undivided cell, electrocatalysis is also involved in the complex PEF process because water can be oxidized on the anode surface to additionally yield heterogeneous hydroxyl radical. In the case of an active IrO_2 anode, physisorbed $IrO_2(^{\cdot}OH)$ is produced as follows [34]:

$$IrO_2 + H_2O \rightarrow IrO_2(^{\cdot}OH) + H^+ + e^- \quad (7)$$

Benzothiazoles (BTs), the most important heterocyclic compounds [35], are high production volume chemicals [36,37] used in industrial and household goods as corrosion inhibitors, photosensitizers and photostabilizers, fungicides or vulcanization accelerators [37]. Children, for example, may undergo direct dermal exposure due to the presence of BTs in clothes [36]. BTs constitute a large group of contaminants of emerging concern (CECs) with frequent occurrence in the environment. They have been detected in 15 rivers in Germany at concentrations ranging from 58 to 856 ng L^{-1} [38], as well as in outdoor air [37]. Their discharge into natural water arises from an incomplete removal in wastewater treatment plants (WWTPs) [39,40]. Two BTs are ubiquitous in the effluents from WWTPs, namely benzothiazole (BTH, C_7H_5NS) and 2-hydroxybenzothiazole (2-OH-BTH, C_7H_5NOS) [41]. Their long lifetime in surface water facilitates their occurrence in tap water at an average value of 406 ng L^{-1} [42] and in human urine at maximal of 9.78 μg L^{-1} for BTH and 4.37 μg L^{-1} for 2-OH-BTH [43]. The inefficacy of WWTPs can be explained from the usually poor biodegradability of BTs. Only some few bacteria in pure cultures showed ability to degrade them [44]. This was confirmed in WWTPs, attaining 46% removal of 2-OH-BTH in anaerobic reactors [45]. Conversely, membrane bioreactors with long-term adaptation were able to reach 96% removal of BTH [46]. BTs may be hazardous even at low exposure dose, as observed either in vitro or in vivo tests [42], causing adverse effects on the liver and kidney, dermatitis and respiratory irritation [36]. BTH and 2-OH-BTH exerted cytotoxicity on rainbow trout [38] and, in general, BTs are associated to carcinogenicity [42], genotoxicity [37,40] and endocrine disruption [37].

Some authors have studied the performance of UVC alone or combined with H_2O_2 [47,48], ozonation [49], photo-Fenton [50], chlorination [51] and activated peroxomonosulfate [52] to degrade BTH. Some of these works also addressed the treatment of 2-OH-BTH [47,51,52] but, surprisingly, the degradation of theses BTs by EAOPs has not been investigated yet.

In this work, the performance of UVA-PEF, UVC-PEF and several part-time or full-time UVA-/UVC-PEF combinations to degrade a mixture of BTH and 2-OH-BTH has been investigated. Electrolytic trials at a constant current density (j) have been carried out in a bench-scale IrO_2/GDE tank reactor to assess the effect of the target pollutants concentration and j on the decay kinetics and total organic carbon (TOC) removal. To explain the benefits of using both UV light sources, the time course of H_2O_2, $^{\cdot}OH$ and Fe^{2+} has been monitored. Finally, the main oxidation products formed during the optimum treatment have been identified.

2. Materials and methods

2.1. Chemicals

Benzothiazole (96% purity) and 2-hydroxybenzothiazole (98% purity) were purchased from Sigma-Aldrich. Analytical grade tartronic, oxalic and oxamic acids were purchased from Panreac. Analytical grade Fe(II) sulfate heptahydrate, Fe(III) chloride and sulfuric acid were purchased from Merck and Sigma-Aldrich. Analytical grade potassium tris(oxalato)ferrate(III) trihydrate for actinometric determination was supplied by Cymit Quimica S.L. Analytical grade Ti(IV) oxysulfate hydrate for H_2O_2 measurements was purchased from Panreac. 1,10-Phenantroline monohydrate (99% purity) for Fe^{2+} determination was supplied by Alfa-Aesar. Analytical grade dimethylsulfoxide (DMSO) and 2,4-dinitrophenylhydrazine (DNPH) for $^{\cdot}OH$ determination were acquired from Sigma-Aldrich. Other chemicals and solvents were of either analytical or high-performance liquid chromatography (HPLC) grade supplied by Merck, Sigma-Aldrich and Panreac. High-purity water from Millipore Milli-Q system (resistivity > 18.2 MΩ cm) was used to prepare solutions.

2.2. Photo-assisted electrolytic trials

All the electrolyses were made in an open, undivided, cylindrical glass tank reactor, under stirring with a magnetic bar at 750 rpm. The treated solution was kept at 25 °C upon recirculation of thermostated water through a jacket surrounding the vessel. The anode was a 3 cm^2 Ti/IrO_2-based plate purchased from NMT Electrodes (Pinetown, South Africa) and the cathode was a 3 cm^2 carbon-PTFE GDE purchased from Sainergy Fuel Cell (Chennai, India). The cathode provided H_2O_2 to the solution in a continuous manner by injecting compressed air at 1 L min^{-1} through the carbon cloth. The two electrodes were mounted as described previously [21], with an interlectrode gap of 1 cm^2. An Amel 2051 potentiostat-galvanostat was used to provide constant j, connected to a Demestres 601BR multimeter to monitor the cell voltage.

Trials were performed with 200 mL of solutions containing one or two BTs, in the presence of 0.050 M Na_2SO_4 as background electrolyte and 0.20 mM $FeSO_4$ as catalyst source at pH 3.0, because this pH is optimal for Fenton's Reaction (1) [16,20,53,54]. In PEF treatments, the solution was irradiated with: (i) UVA light (λ_{max} = 360 nm) from a 6-W Philips TL/6 W/08 fluorescent black light blue tube and/or (ii) UVC light (λ_{max} = 254 nm) from an 8-W Philips T5/8 W fluorescent tube. They were placed on top of the electrochemical reactor, at a distance of 13 cm from the solution surface. To better collect the UV photons, the reactor was placed in a mirror box. A sketch of the experimental setup can be seen in Fig. S1.

2.3. Apparatus and analytical methods

Chemical actinometry using ferrioxalate as actinometer was conducted to quantify the actual light intensity absorbed by the solution upon irradiation with the UVA and UVC lamps [55]. A 200 mL solution of 6 mM ferrioxalate was introduced in the electrochemical reactor equipped with the IrO_2-based anode and GDE to mimic the PEF assays, and the absorbance measurements were made at λ = 510 nm on a Shimadzu 1800 UV/Vis spectrophotometer. The photon flux and irradiance obtained are collected in Table S1, where greater values, as expected, resulted under UVC irradiation. It can be observed that the

reflection ratio ($E_{\text{with mirrors}}$ / $E_{\text{without mirrors}}$) was greater than 30% in both cases, which justifies the use of the mirror box (see Fig. S1) since it enhances the performance of the PEF treatments.

The solution pH was monitored with a Crison GLP 22 pH-meter. After withdrawal from the treated solution, each sample was microfiltered with a Whatman 0.45 μm PTFE filter before analysis. TOC was measured on a Shimadzu TOC-VCSN analyzer, using the non-purgeable organic content (NPOC) method, yielding a reproducibility of ± 1%. From these data, the mineralization current efficiency (MCE), as a percentage, for each assay at current I (A) and electrolysis time t (h) was then estimated as [56]:

$$\%\,\text{MCE} = \frac{n_{\text{mean}} FV\Delta(\text{TOC})}{4.32 \times 10^7 m_{\text{mean}} It} 100 \quad (8)$$

where n_{mean} is the mean number of consumed electrons, F is the Faraday constant (96,485 C mol^{-1}), V is the solution volume (L), $\triangle$(TOC) is the TOC decay (mg L^{-1}), 4.32×10^7 is a conversion factor and m_{mean} is the mean number of the C atoms in the treated solutions.

Two main contributions to energy consumption per unit TOC mass were determined in all PEF treatments: the electrochemical one ($(EC_{TOC})_{electro}$), resulting from the electric energy consumption of the power supply needed to run the electrolyses, and the photochemical one ($(EC_{TOC})_{photo}$) that depended on the lamp power. Their values were determined from Eqs. (9) [32,54] and (10), respectively:

$$(EC_{TOC})_{electro}\ (\text{kWh}\ (\text{g TOC})^{-1}) = \frac{E_{cell} It}{V\Delta\text{TOC}} \quad (9)$$

$$(EC_{TOC})_{photo}\ (\text{kWh}\ (\text{g TOC})^{-1}) = \frac{Pt}{V\Delta\text{TOC}} \quad (10)$$

where E_{cell} denotes the average cell voltage (V), P the nominal lamp power (W) and the rest of parameters have been defined above. The E_{cell} values using the IrO_2-based/GDE cell were 3.3, 5.1 and 8.4 V at 15.0, 33.3 and 60.0 mA cm^{-2}, respectively. The total energy consumption per unit TOC mass ($(EC_{TOC})_{total}$) was then calculated as sum of $(EC_{TOC})_{electro}$ and $(EC_{TOC})_{photo}$.

The concentration of each benzothiazole during the electrolysis was determined by reversed-phase HPLC using a Waters system composed of a 600 chromatograph fitted with a BDS Hypersil C18 5 μm column (250 mm × 4.6 mm), kept at 35 °C and coupled to a Waters 996 photodiode array detector (PAD) set at 254 nm. The mobile phase was a 50:50 (v/v) CH_3CN/10 mM KH_2PO_4 (pH 3.0) mixture eluted at 1.0 mL min^{-1}. The retention time for 2-OH-BTH and BTH was 4.6 and 5.5 min, respectively. Samples were previously diluted with CH_3CN to stop the degradation process. The resulting carboxylic acids were analyzed by ion-exclusion HPLC using the same apparatus but fitted with a Bio-Rad Aminex HPX 87H column (300 mm × 7.8 mm) at 35 °C and the PDA detector set at λ = 210 nm. Chromatograms were recorded by eluting 4 mM H_2SO_4 at 0.6 mL min^{-1} and defined peaks for oxalic, tartronic and oxamic acids appeared at 7.0, 8.0 and 9.8 min, respectively.

Ammonium ion concentration was determined spectrophotometrically according to the indophenol blue method [24]. The concentrations of sulfate, nitrite and nitrate ions were obtained by ion chromatography using a Shimadzu 10Avp LC fitted with a Shim-Pack IC-A1S column (100 mm × 4.6 mm) at 40 °C and coupled to a Shimadzu CDD 10Avp conductivity detector. A solution composed of 2.4 mM tris (hydroxymethyl)aminomethane (pH 4.0) and 2.6 mM phthalic acid was eluted at 1.5 mL min^{-1} as mobile phase. The concentration of H_2O_2 accumulated in the medium was obtained from the absorbance of its yellow complex with Ti(IV) at λ = 408 nm, measured on the above spectrophotometer [57]. The dissolved Fe^{2+} content was obtained from the absorbance of its reddish complex formed with 1,10-phenantroline at λ = 510 nm using the same equipment. The $^{\cdot}OH$ concentration was quantified by DMSO trapping [58]. For this, the same electrochemical reactor and electrodes were employed, but replacing the pollutant solution by a 250 mM DMSO solution. In brief, formaldehyde was quantitatively generated, which then reacted with 6 mM DNPH in a phosphate buffer medium at pH 4.0 to form the corresponding hydrazine (HCHO–DNPH), then being analyzed by reversed-phase HPLC with the above equipment. A 50:50 (v/v) CH_3CN/H_2O (pH 3.0) mixture was used as mobile phase at 1.0 mL min^{-1} and the PDA was selected at λ = 355 nm, yielding a peak at 8.3 min. The detection limit for hydroxyl radical was 1.17 μM.

Average results from duplicate trials are always reported and error bars (95% confidence interval) are shown in all figures.

Stable heteroaromatic reaction products were detected from the treatment of 200 mL of 20 mg L^{-1} BTH, 20 mg L^{-1} 2-OH-BTH and 20 mg L^{-1} BTH + 20 mg L^{-1} 2-OH-BTH solutions by UVA-PEF and UVA-/UVC-PEF at 33.3 mA cm^{-2}. The organic components accumulated in each treated solution were extracted with CH_2Cl_2 and further, the resulting organic solution was dried over Na_2SO_4, filtered and concentrated to be analyzed by gas chromatography-mass spectrometry (GC–MS), using the NIST05 MS database for mass spectra identification. The analysis was made with an Agilent Technologies system composed of a 6890 N chromatograph, equipped with a nonpolar Teknokroma Sapiens-X5 ms 0.25 μm column (30 m × 0.25 mm) and coupled to a 5975C mass spectrometer operating in EI mode at 70 eV. The temperature ramp was initiated at 36 °C, reaching 320 °C at a heating rate of 5 °C min^{-1}. The temperature of the inlet, source and transfer line was 250, 230 and 300 °C.

3. Results and discussion

3.1. Degradation of each benzothiazole in their mixtures by PEF with UVA or UVC light

First assays were made by electrolyzing 200 mL of mixtures containing 20 mg L^{-1} BTH + 20 mg L^{-1} 2-OH-BTH in 0.050 M Na_2SO_4 with 0.20 mM Fe^{2+}, at pH 3.0 and 25 °C using an IrO_2-based/GDE cell under PEF conditions. The concentration decay of each compound was assessed at different j values ranging from 15.0 to 60.0 mA cm^{-2}. No significant changes in pH were found during these trials, remaining quite stable at ca. 3.0. Fig. 1a and b shows a slower abatement of 2-OH-BTH content. A plausible explanation is that this molecule was not only degraded, as occurred with BTH, but it was simultaneously produced upon hydroxylation of this latter pollutant, as will be discussed below, thus decelerating the overall removal of 2-OH-BTH. On the other hand, the decays became slightly faster when replacing UVA by UVC light and as j was increased. In UVC-PEF process, BTH disappeared at shorter times of 40, 30 and 25 min at raising j of 15.0, 33.3 and 60.0 mA cm^{-2}, respectively, whereas 2-OH-BTH was reduced by 89% after 40 min at 15.0 mA cm^{-2}, being completely removed after 35 min at 33.3 mA cm^{-2} and 25 min at 60.0 mA cm^{-2}. The rapid decay of both target molecules regardless of the lamp employed suggests that, within such short treatment times, the pre-eminent degradation mechanism involved the attack of homogeneous $^{\cdot}OH$ formed from Fenton's Reaction (1). The contribution of this oxidant became even more relevant as j was raised, owing to the concomitant acceleration of Reaction (2) that led to a higher H_2O_2 production [3,5,23]. However, no higher j values were tested because this would cause a much greater energy consumption associated with a relative larger destruction of $^{\cdot}OH$ via parasitic reactions [3,4]. Other less relevant degradation mechanisms entailed the destruction of pollutants by: (i) heterogeneous $IrO_2(^{\cdot}OH)$ originated from Reaction (7), whose oxidation power is assumed to be rather low [34,59]; (ii) $^{\cdot}OH$ arising from the photolytic H_2O_2 homolysis, which would require the accumulation of enough H_2O_2 for a longer time to be more evident; (iii) the occurrence of photo-Fenton Reaction (3), which also needs a long time to show up [18]; and (iv) direct UV photolysis [47,48]. The high ability of the GDE to accumulate H_2O_2, alongside the aromatic nature of both pollutants with absorption bands in the UVC range, justify the slight superiority of UVC-PEF.

The good linear fittings obtained from a pseudo-first-order kinetic

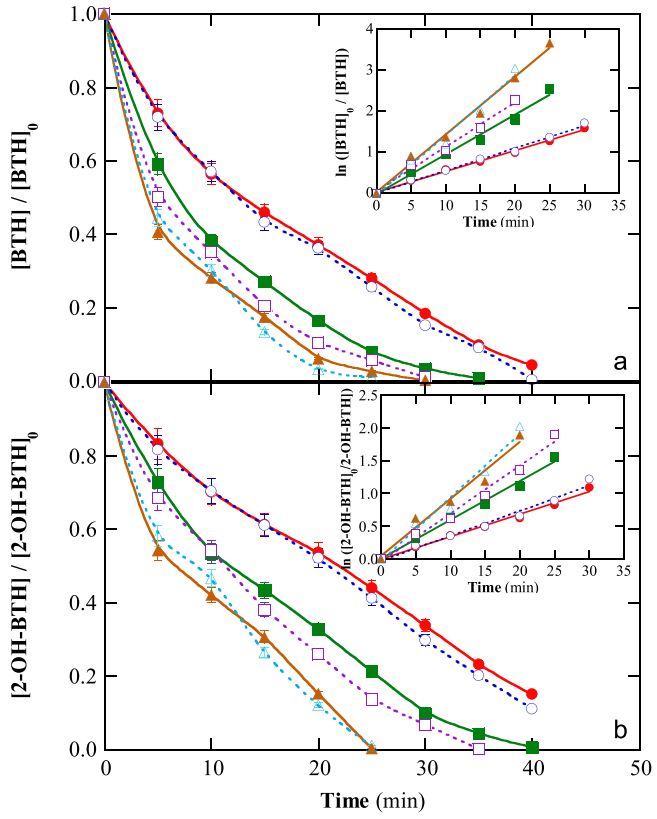

Fig. 1. Effect of current density and irradiation source on the change of the normalized concentration of (a) benzothiazole (BTH) and (b) 2-hydroxybenzothiazole (2-OH-BTH) with electrolysis time for the PEF treatment of 200 mL of 20 mg L^{-1} BTH +20 mg L^{-1} 2-OH-BTH in 0.050 M Na_2SO_4 with 0.20 mM Fe^{2+}, at pH 3.0 and 25 °C using an IrO_2-based/GDE cell. Current density: (●,○) 15.0 mA cm^{-2}, (■,□) 33.3 mA cm^{-2} and (▲,△) 60.0 mA cm^{-2}. UV lamp: (●,■,▲) 6-W UVA and (○,□,△) 8-W UVC. The insets present the pseudo-first-order kinetic analysis of the concentration decays.

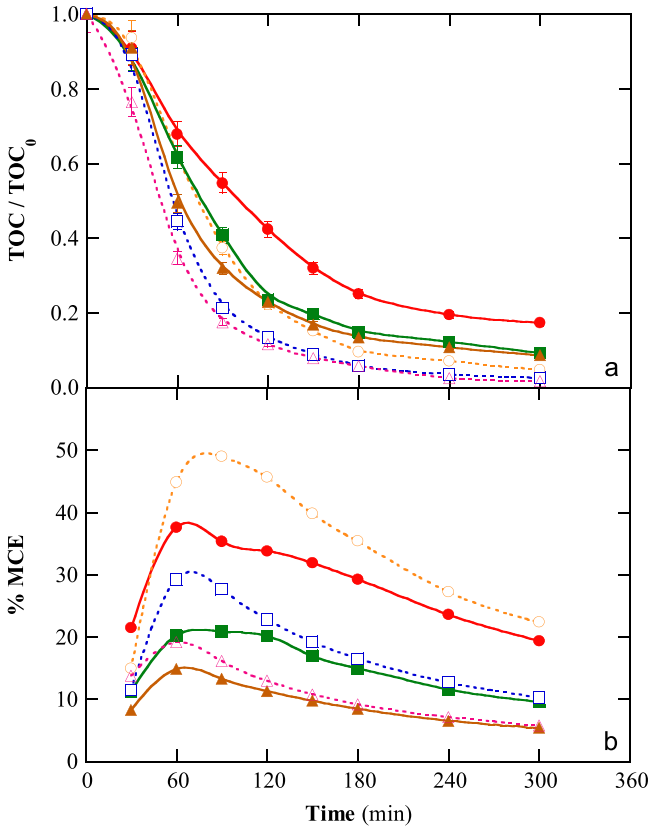

Fig. 2. Effect of current density and irradiation source on (a) normalized TOC and (b) mineralization current efficiency vs. electrolysis time for the PEF treatment of 200 mL of 20 mg L^{-1} BTH +20 mg L^{-1} 2-OH-BTH (i.e., 23.6 mg L^{-1} TOC) in 0.050 M Na_2SO_4 with 0.20 mM Fe^{2+}, at pH 3.0 and 25 °C employing the IrO_2-based/GDE cell. Current density: (●,○) 15.0 mA cm^{-2}, (■,□) 33.3 mA cm^{-2} and (▲,△) 60.0 mA cm^{-2}. Lamp: (●,■,▲) 6-W UVA and (○,□,△) full-time 6-W UVA / 8-W UVC.

analysis of the concentration data of Fig. 1a and b are presented in their inset panels. The apparent rate constant (k_1) for BTH degradation in UVC-PEF increased as: 0.055 min^{-1} (R^2 = 0.993) at 15.0 mA cm^{-2}, 0.109 min^{-1} (R^2 = 0.988) at 33.3 mA cm^{-2} and 0.146 min^{-1} (R^2 = 0.983) at 60.0 mA cm^{-2}. Slightly lower k_1-values of 0.051 min^{-1} (R^2 = 0.995), 0.097 min^{-1} (R^2 = 0.988) and 0.141 min^{-1} (R^2 = 0.990) were found in UVA-PEF. The slower removals of 2-OH-BTH mentioned above were consistent with k_1-values of 0.038 min^{-1} (R^2 = 0.980), 0.073 min^{-1} (R^2 = 0.985) and 0.089 min^{-1} (R^2 = 0.975) in UVC-PEF, being 0.034 min^{-1} (R^2 = 0.989), 0.059 min^{-1} (R^2 = 0.991) and 0.095 min^{-1} (R^2 = 0.980) in UVA-PEF. Such linear profiles can be associated with the availability of a constant amount of reactive ·OH at each j value, in agreement with the second-order rate constants reported at pH 7.0 for BTH ((8.61 ± 0.23)×10^9 M^{-1} s^{-1}) and 2-OH-BTH ((5.08 ± 0.44)×10^9 M^{-1} s^{-1}). These values were determined by competition kinetics method during the UVC/H_2O_2 treatment of solutions containing 1 μM of the given pollutant [47].

3.2. Mineralization of mixtures of benzothiazoles by PEF with UVA and UVA/UVC light

The mineralization of mixtures of 20 mg L^{-1} BTH +20 mg L^{-1} 2-OH-BTH by UVA-PEF and full-time UVA-/UVC-PEF at different j values was monitored from their TOC abatement for 300 min. A continuous TOC decay during the whole trials is depicted in Fig. 2a. In both EAOPs, a markedly higher mineralization rate was obtained as j was increased, with a more significant acceleration in the case of UVA-/UVC-PEF. In this treatment, an almost total mineralization between 95.3% and 98.4% was finally attained, as can be confirmed from data summarized in Table 1. Conversely, a partial mineralization with much lower TOC reduction, between 82.7% and 91.4%, was achieved in UVA-PEF (see Table 1). In both methods, the TOC decay profiles observed in Fig. 2a at 33.3 and 60.0 mA cm^{-2} from 90 min of electrolysis were analogous and hence, a j = 33.3 mA cm^{-2} was set for subsequent trials. The enhanced mineralization reached when changing from 15.0 to 33.3 mA cm^{-2} was due to the greater production of ·OH from Reactions (1) and/or (5), which resulted from the larger H_2O_2 generation. Those numerous radicals destroyed a greater amount of organic intermediates, eventually increasing the content of photoactive products that could be more rapidly photolyzed under UV light. This behavior was also verified when j rose to 60.0 mA cm^{-2}, but for 90 min, whereupon the concentration of recalcitrant products was similar to that accumulated at 33.3 mA cm^{-2}, further being removed at the same rate. This suggests that, at long times, the degradation was limited by the slow reaction between stable organics and ·OH, mainly produced by Reaction (5) since H_2O_2 attained its greater content at that stage (see below). The clear superiority of UVA-/UVC-PEF over UVA-PEF can then be ascribed to the larger photolytic ability of UVC light. Note that Borowska et al. [48] reported the overall removal of 10 mg L^{-1} BTH at pH 5.0 after about 25 min of UVC/H_2O_2 treatment with a 200-W lamp and 30 mg L^{-1} H_2O_2, but without significant TOC removal. Hence, the mineralization of benzothiazoles in PEF can be mainly explained by the reaction of products with ·OH formed from Fenton's Reaction (1), along with their photodegradation under UVA and/or UVC light.

The fate of the heteroatoms (S and N) of both BTs was ascertained

Table 1
Percentage of TOC removal and mineralization current efficiency, along with electrochemical, photochemical and total energy consumptions per unit TOC mass determined for the PEF treatment of 200 mL of various mixtures of BTH and 2-OH-BTH in 0.050 M Na_2SO_4 with 0.20 mM Fe^{2+}, at pH 3.0 and 25 °C using an IrO_2-based/GDE cell at selected conditions.

j[a] (mA cm^{-2})	Time of 6-W UVA (min)	Time of 8-W UVC (min)	% TOC removal	% MCE	$(EC_{TOC})_{electro}$ (kWh (g TOC)$^{-1}$)	$(EC_{TOC})_{photo}$ (kWh (g TOC)$^{-1}$)	$(EC_{TOC})_{total}$ (kWh (g TOC)$^{-1}$)
40 mg L^{-1} BTH + 40 mg L^{-1} 2-OH-BTH							
33.3	300	–	90.7	19.1	0.299	3.509	3.808
33.3	300	Last 150	97.5	20.6	0.278	5.441	5.719
20 mg L^{-1} BTH + 20 mg L^{-1} 2-OH-BTH							
15.0	300	–	82.7	19.4	0.191	7.699	7.890
15.0	300	300	95.3	22.3	0.164	15.427	15.591
33.3	300	–	90.8	9.6	0.596	7.012	7.608
33.3	300	Last 60	95.3	10.0	0.568	8.461	9.029
33.3	300	Last 120	97.5	10.3	0.555	10.012	10.567
33.3	300	Last 180	98.0	10.3	0.552	11.694	12.246
33.3	300	300	97.5	10.3	0.555	15.237	15.792
33.3	–	300	96.3	10.2	0.562	8.815	9.377
60.0	300	–	91.4	5.3	1.758	6.966	8.724
60.0	300	300	98.4	5.8	1.633	15.097	16.730
10 mg L^{-1} BTH + 10 mg L^{-1} 2-OH-BTH							
33.3	300	–	88.3	4.6	1.229	14.420	15.649
33.3	300	Last 150	97.0	5.1	1.118	22.554	23.672

[a] Current density.

by measuring the concentration of inorganic ions released from the above mixtures during the UVA-/UVC-PEF treatment. All the initial S (8.98 mg L^{-1}) was transformed into SO_4^{2-} ion, whereas the initial N (3.92 mg L^{-1}) was pre-eminently converted into NH_4^+ ion without accumulation of NO_2^- and NO_3^- ions. Fig. S2 depicts the time course of the concentration of NH_4^+ produced, which attained a final value of 4.09 mg L^{-1} (81.1% of initial N). Considering that 97.5% of mineralization was reached at that time, one can infer that total N was partly lost as volatile species like N_2 and N_xO_y, as reported for other *N*-containing target pollutants [3,5,21]. According to these results, the theoretical overall mineralization of BTH and 2-OH-BTH can be expressed from Reactions (11) and (12), with a number of consumed electrons n (BTH) = 36 and n(2-OH-BTH) = 34, respectively:

$$C_7H_5NS + 18H_2O \rightarrow 7CO_2 + NH_4^+ + SO_4^{2-} + 37H^+ + 36e^- \quad (11)$$

$$C_7H_5NOS + 17H_2O \rightarrow 7CO_2 + NH_4^+ + SO_4^{2-} + 35H^+ + 34e^- \quad (12)$$

Taking into account the molar fractions of both BTs, i.e., x(BTH) and x(2-OH-BTH), one can then assume that the mixtures were mineralized with n_{mean} = (x(BTH) × n(BTH)) + (x(2-OH-BTH) × n(2-OH-BTH)) = (0.528 × 36) + (0.472 × 34) = 35.06, and m_{mean} = 7.

Fig. 2b shows the MCE values determined for the assays of Fig. 2a using Eq. (8) with the above n_{mean} and m_{mean} values. As can be seen, the mineralization current efficiency decreased strongly with raising j, being always greater in UVA-/UVC-PEF treatments. These tendencies can also be noted in Table 1, where the MCE values after 300 min of electrolysis are listed for both processes. In the most efficient one, a maximum MCE of 49.0% was reached at 90 min, further drastically dropping down to 22.3%. This volcano-shaped curve can be observed in all cases in Fig. 2b, being typical in EAOPs [3]. The MCE decrease at long time can be ascribed to both, mass transport limitations once the organic load has been quantitatively removed and the increasing recalcitrance of by-products to oxidation [3,34].

Table 1 collects the three types of EC_{TOC} values at the end of the experiments of Fig. 2a. The $(EC_{TOC})_{electro}$ contribution grew progressively with increasing j owing to the remarkable rise of E_{cell}. Nonetheless, this parameter was always much smaller than $(EC_{TOC})_{photo}$, which in turn was much greater in UVA-/UVC-PEF as compared to UVA-PEF despite the higher mineralization achieved. At 33.3 mA cm^{-2}, for example, $(EC_{TOC})_{electro}$ represented only a 7.8% of $(EC_{TOC})_{total}$ in the case of UVA-PEF, decreasing to 3.5% in UVA-/UVC-PEF, whereas the $(EC_{TOC})_{total}$ in the former treatment was almost halved.

3.3. On the positive effect of UVC light in UVA-PEF treatment

The influence of UVC light in a hybrid treatment with UVA-PEF was investigated by switching on the UVC lamp at different electrolysis times during the treatment of 200 mL of 20 mg L^{-1} BTH + 20 mg L^{-1} 2-OH-BTH in 0.050 M Na_2SO_4 with 0.20 mM Fe^{2+}, at pH 3.0, 25 °C and 33.3 mA cm^{-2}. Fig. 3a depicts the normalized TOC-time curves obtained. UVA-PEF yielded the slowest mineralization, attaining 90.8% TOC abatement at 300 min, whereas the fastest TOC decay ending in 97.5% removal was achieved in full-time UVA-/UVC-PEF. In UVC-PEF, the rate was in between the other two, reaching 96.3% mineralization. When part-time UVC-PEF was combined with UVA-PEF, the mineralization was accelerated. The profile became gradually closer to that obtained in full-time UVA-/UVC-PEF profile, attaining final TOC reductions of 97.5–98.0% when the UVC photons were irradiated during the last 120–180 min (see Table 1). This behavior can also be inferred from the corresponding MCE-time curves depicted in Fig. 3b, as well as from final MCE values listed in Table 1.

The aforementioned results demonstrate that UVC radiation is not really needed during the whole electrolysis to achieve the greatest mineralization, but an exposure of solutions to UVC light after approximately 150 min of UVA-PEF is enough, reaching ≥97.0% TOC reduction. This confirms that the main role of UVC photons in UVA-/UVC-PEF is related to the additional generation of $^{\cdot}OH$ from H_2O_2 homolysis via Reaction (5). H_2O_2 is more largely accumulated at long electrolysis time, and the resulting $^{\cdot}OH$ contribute decisively to the destruction of final recalcitrant products favoring their mineralization. Worth noting, the part-time use of the UVC lamp allows minimizing the energy consumption of the treatment thanks to the decrease of $(EC_{TOC})_{photo}$ (see Table 1). As a result, for example, in UVA-/UVC-PEF with UVC employed during the last 120 min, the $(EC_{TOC})_{total}$ was around 33% lower than that required in full-time UVA-/UVC-PEF.

Once concluded that UVA-/UVC-PEF with the UVC lamp used during the last 150 min, operating at 33.3 mA cm^{-2}, was the optimum PEF treatment, its oxidation ability was assessed with different mixtures of both BTs to study the influence of the organic load on the mineralization process. As can be seen in Fig. 4a, the normalized TOC abatement was much slower using solutions with 40 mg L^{-1} BTH + 40 mg L^{-1} 2-OH-BTH than 10 mg L^{-1} BTH + 10 mg L^{-1} 2-OH-BTH. This can be related to the fact that a similar amount of oxidizing agents

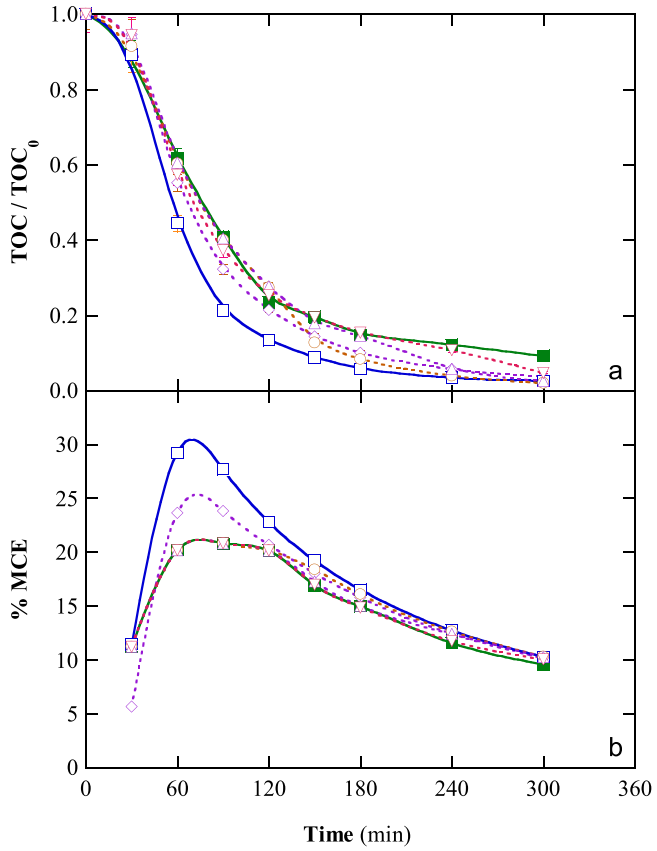

Fig. 3. Influence of irradiation source on the variation of (a) normalized TOC and (b) mineralization current efficiency with electrolysis time for the PEF treatment of 200 mL of a mixture of 20 mg L^{-1} BTH + 20 mg L^{-1} 2-OH-BTH in 0.050 M Na_2SO_4 with 0.20 mM Fe^{2+}, at pH 3.0 and 25 °C using the IrO_2-based/GDE cell at 33.3 mA cm^{-2}. Lamp arrangement: (■) 6-W UVA, (◇) 8-W UVC, (▽) 6-W UVA/8-W UVC (last 60 min), (△) 6-W UVA / 8-W UVC (last 120 min), (○) 6-W UVA/8-W UVC (last 180 min) and (□) full-time 6-W UVA / 8-W UVC.

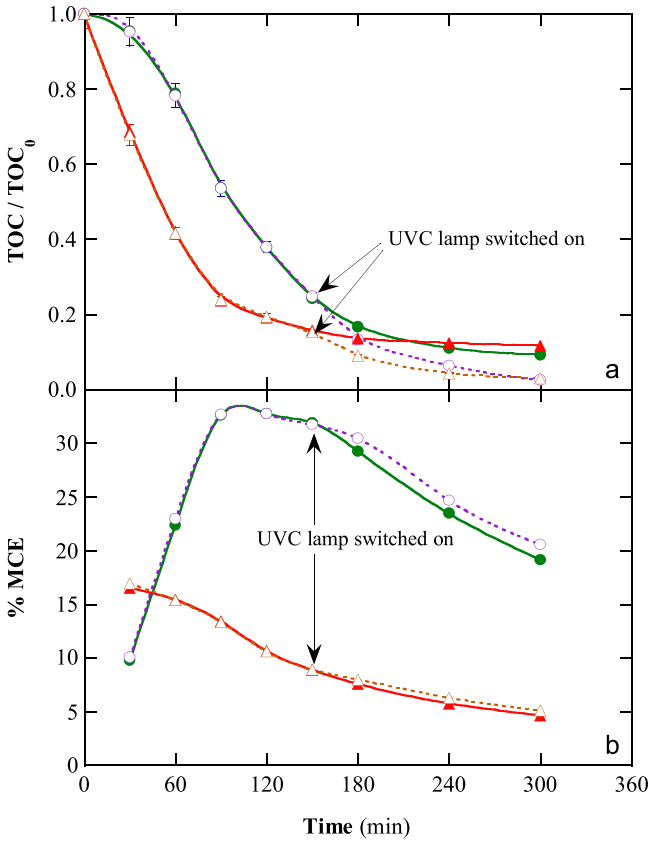

Fig. 4. Effect of substrate content and irradiation source on (a) normalized TOC and (b) mineralization current efficiency with electrolysis time for the PEF treatment of 200 mL of mixtures of BTH and 2-OH-BTH in 0.050 M Na_2SO_4 with 0.20 mM Fe^{2+}, at pH 3.0 and 25 °C using the IrO_2-based/GDE cell at 33.3 mA cm^{-2}. Mixture: (■,■) 10 mg L^{-1} BTH + 10 mg L^{-1} 2-OH-BTH and (■,□) 40 mg L^{-1} BTH + 40 mg L^{-1} 2-OH-BTH. Lamp arrangement: (■,■) 6-W UVA and (■,□) 6-W UVA / 8-W UVC (last 150 min).

is expected to be produced in both cases and hence, they mineralize more rapidly the latter mixture because of the smaller number of organic molecules. It is noticeable the large acceleration of TOC removal once the UVC lamp was switched, thereby reaching an almost total mineralization (≥97.0%) in both cases, which clearly upgraded the removals around 88.3–90.7% achieved in UVA-PEF (see Table 1). This is analogous to the trends described above for the 20 mg L^{-1} BTH + 20 mg L^{-1} 2-OH-BTH mixture under similar conditions (see Fig. 3a and Table 1). As a result of the enhanced mineralization during the last 150 min, the MCE values were upgraded, as shown in Fig. 4b. Furthermore, the data in that figure and Table 1 reveal a gradual rise of MCE at increasing content of both BTs. Using the 40 mg L^{-1} BTH + 40 mg L^{-1} 2-OH-BTH mixture, the maximum value of 32.8% was obtained at 120 min, further decaying to 20.6% due to the previously explained phenomena. The lower efficiencies at smaller organic loads are typical in EAOPs, which is explained by the relative decrease of available ·OH because of the enhancement of their waste reactions, involving, for example, their reaction with H_2O_2 to yield $HO_2^{\cdot -}$ from Reaction (6) or their dimerization to form H_2O_2 [3,32]. Table 1 shows that the use of UVC light during the last 150 min for 40 mg L^{-1} BTH + 40 mg L^{-1} 2-OH-BTH entailed the lowest $(EC_{TOC})_{total}$ among all part-time treatments (5.719 kW h (g TOC)$^{-1}$). It was higher than 3.808 kW h (g TOC)$^{-1}$ found for the UVA-PEF process, but the latter yielded a significantly lower mineralization (90.7% vs. 97.5%), which is dangerous due to the potential presence of toxic organic by-products.

3.4. Evolution of generated H_2O_2 and ·OH

Blank experiments were performed in order to elucidate the evolution of generated H_2O_2 and ·OH under the tested experimental conditions. The treatment of 200 mL of 0.050 M Na_2SO_4 at pH 3.0, 25 °C and 33.3 mA cm^{-2} by electrochemical oxidation with electrogenerated H_2O_2 (EO-H_2O_2) yielded a gradual increase in H_2O_2 concentration up to a maximal of 25.5 mM from 180 min. Fig. 5a shows a similar evolution, but with smaller H_2O_2 accumulation, upon UVC irradiation, attaining a steady value around 13 mM. In these assays, the plateau was reached once the H_2O_2 generation rate from Reaction (2) became equal to its destruction one. The latter was mainly due to its oxidation to O_2 at the IrO_2-based anode surface [3,18], along with its photolysis via Reaction (5) in UVC-EO-H_2O_2. The destruction of H_2O_2 was strongly promoted in the presence of 0.20 mM Fe^{2+}, especially upon irradiation with UVA light due to the predominance of Fenton's Reaction (1) and the photoregeneration of Fe^{2+} via photo-Fenton Reaction (3). Fig. 5a highlights the lower H_2O_2 accumulation at the end of this UVA-PEF treatment, i.e., 5.7 mM, as compared to EO-H_2O_2. The illumination of the solution with UVC light caused an additional decrease of H_2O_2 final content, as shown in Fig. 5a. Similar quasi-steady concentrations between 3.2 and 3.6 mM were attained after 300 min of UVC-PEF, full-time UVA-/UVC-PEF and part-time UVA-/UVC-PEF (with UVC lamp switched on at 150 min) treatments. This confirms the important role of photolytic H_2O_2 homolysis in all UVC-assisted PEF treatments.

The production of ·OH during the UVA-PEF and UVC-PEF treatments of 20 mg L^{-1} BTH + 20 mg L^{-1} 2-OH-BTH mixtures under the

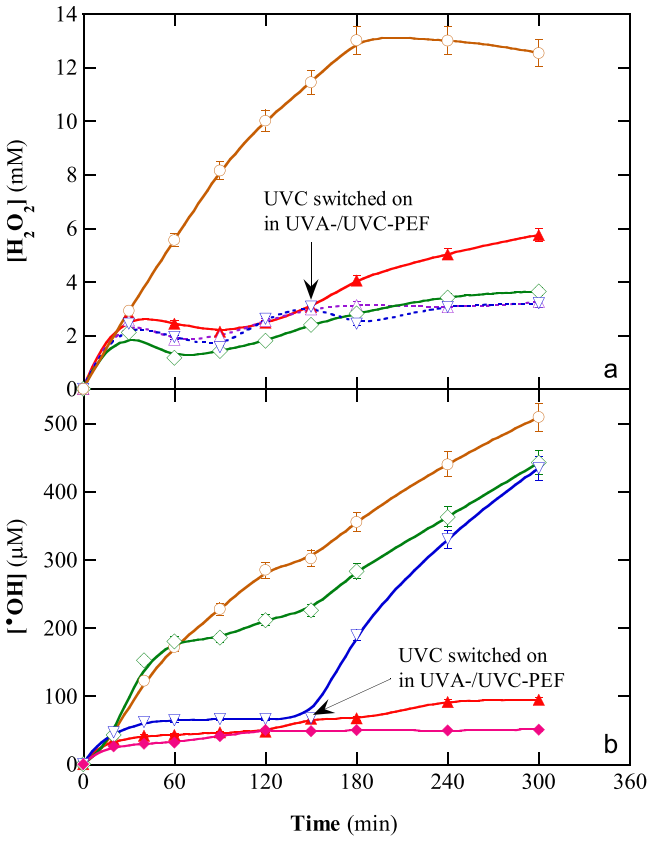

Fig. 5. Concentration of (a) H_2O_2 accumulated and (b) ˙OH produced vs. electrolysis time for the electrolysis of 200 mL of 0.050 M Na_2SO_4 with 0.20 mM Fe^{2+}, at pH 3.0 and 25 °C using the IrO_2-based/GDE cell at 33.3 mA cm^{-2}. Method: (□) EO-H_2O_2 (without Fe^{2+} catalyst) under irradiation with an 8-W UVC lamp, (●) EF (without irradiation) and PEF with (■) 6-W UVA, (△) 8-W UVC, (⊕) full-time 6-W UVA/8-W UVC and (▼) 6-W UVA/8-W UVC (last 150 min) lamps.

conditions of Fig. 1a and b was assessed by addition of 100 mM *t*-butanol, a known scavenger of this radical. Compared with the data of Fig. 1, Fig. S3 depicts a drastic inhibition of BTH abatement. This pollutant was reduced by only 10.0% under UVA irradiation, slightly rising up to 14.1% using UVC light for 60 min of electrolysis. A slower decrease can be observed for 2-OH-BTH, which was only reduced by 6.6% and 9.5%, respectively, because of its co-generation during BTH degradation, as hypothesized above. These findings confirm the preponderant role of ˙OH during PEF treatments. The slightly larger decays of both BTs upon illumination with UVC photons can then be related to their simultaneous direct photodecomposition [47,48].

Fig. 5b shows the ˙OH concentration rising steadily with time, at least during the first minutes in all cases, which can be related to the H_2O_2 accumulation profiles shown in Fig. 5a. The lowest amount of ˙OH was formed under EF conditions, as a result of Fenton's Reaction (1) between generated H_2O_2 and added Fe^{2+}. This value was slightly upgraded in UVA-PEF due to the additional Fe^{2+} regeneration from photolytic Reaction (3), with the consequent acceleration of Reaction (1). It can be seen that the exposure to UVC light caused a dramatic enhancement of ˙OH generation, owing to the photolytic homolysis of H_2O_2 via Reaction (5). The ˙OH production decreased in the order: EO-H_2O_2 with UVC > full-time UVA-/UVC-PEF > UVA-/UVC-PEF (UVC irradiation during the last 150 min). The smaller yield in the second process as compared to the former one can be explained by the partial decomposition of H_2O_2 by Fe^{2+} according to Fenton's Reaction (1), which only yields one radical instead of two. Note that the part-time use of UVC light combined with UVA practically produced the

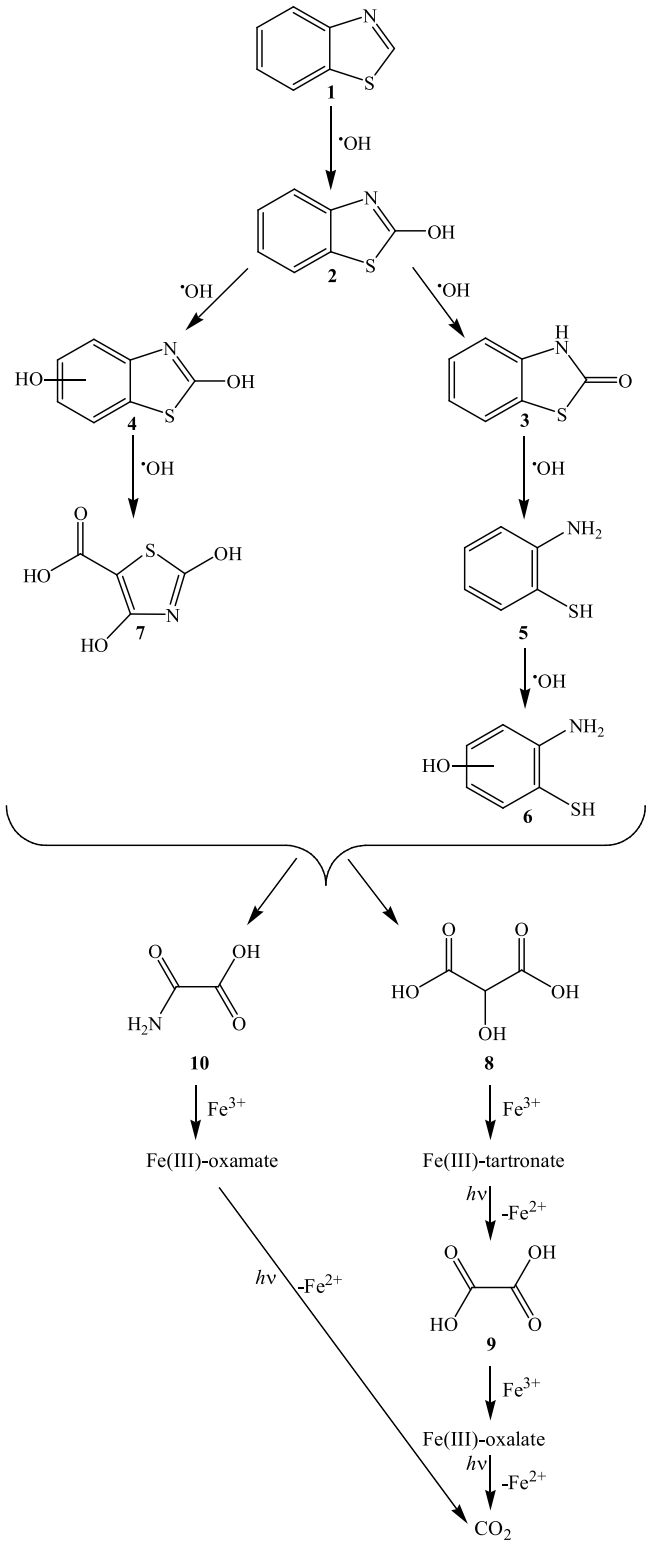

Fig. 6. Proposed reaction pathways for the mineralization of BTH (**1**) by PEF process.

same quantity of ˙OH as the one determined at the end of full-time UVA-/UVC-PEF. This corroborates the positive effect of UVC and justifies its part-time application, as pointed out above. The evident contribution of UVC light to ˙OH production could be considered as not so impressive in terms of TOC abatement (Fig. 4a). However, its action over traces of potentially toxic organic products, thus ensuring the overall mineralization, was crucial.

3.5. Detection of heteroaromatic products and final carboxylic acids

GC–MS analysis of a 20 mg L^{-1} BTH solution treated by UVA-PEF and full-time UVA-/UVC-PEF at 33.3 mA cm^{-2} revealed the generation of 2-OH-BTH as primary product, which confirms the hypothesis made from Fig. 1a and b as well as Fig. S3 to explain the faster removal of BTH. The other detected heteroaromatic products were the same as those found during the electrolysis of 20 mg L^{-1} 2-OH-BTH and 20 mg L^{-1} BTH + 20 mg L^{-1} 2-OH-BTH solutions under similar conditions. Table S2 summarizes the characteristics of the products identified. Based on these compounds, the initial degradation route of BTH (**1**) is proposed in Fig. 6, being valid for all the PEF processes tested and involving ˙OH as the main oxidizing agent. The degradation is initiated by the hydroxylation of the C(2) of BTH (**1**) to yield 2-OH-BTH (**2**), which subsequently can be either oxidized to yield 3H-1,3-benzothiazol-2-one (**3**) or further hydroxylated on the benzene ring to form **4**. The oxidation of **3** causes the cleavage of the thiazole ring, with formation of 2-aminobenzenethiol (**5**). Subsequent hydroxylation of **5** produces the compound **6**. On the other hand, the oxidation of **4** yields 2,5-dihydroxy-1,3-thiazole-4-carboxylic acid (**7**) with cleavage of the benzene ring. The formation of compounds **3** and **5** has also been reported for the degradation of **2** using peroxomonosulfate as the oxidant [52].

The mineralization of benzene rings typically produces short-chain linear carboxylic acids [3–5,18]. This possibility was explored by ion-exclusion HPLC for the 20 mg L^{-1} BTH + 20 mg L^{-1} 2-OH-BTH mixture treated by UVA-PEF, UVC-PEF and UVA-/UVC-PEF (UVC lamp switched on during the last 150 min). Three carboxylic acids, namely tartronic (**8**), oxalic (**9**) and oxamic (**10**), were detected in all cases. It is expected that the former acid is mainly converted into oxalic acid, whereas oxamic acid arises from the oxidation of longer N-derivatives. Under the tested conditions, all these acids form Fe(III)-complexes that are expected to be gradually photolyzed under UVA or UVC irradiation via Reaction (4) [18,26]. Fig. 6 shows the transformation of these acids prior to overall conversion into CO_2.

Fig. 7a–c shows the evolution of these acids in each treatment. It can be observed that all the acids were accumulated more largely in the presence of UVA photons; the greater photon flux and irradiance upon use of UVC light ensured the faster photolysis of the Fe(III)-complexes (see Table S1). The complexes of tartronic and oxamic acids were more persistent, being much quicker the photolysis of Fe(III)-oxalate complexes. All these species were completely photolyzed at the end of the electrolyses. Nevertheless, large amounts of these acids were found at short electrolysis times, suggesting a quick destruction of the heteroaromatic products. At 60 min, for example, 13.1, 18.4 and 5.9 mg L^{-1} of tartronic, oxalic and oxamic acids were determined in the solutions treated either by UVA-PEF or UVA-/UVC-PEF, accounting for 71.2% of the measured TOC (i.e., 14.6 mg L^{-1}, see Fig. 3a). In the UVC-PEF treatment, the concentration of these acids was 6.9, 11.2 and 4.2 mg L^{-1}, i.e., 48.5% of measured TOC. At 300 min, a residual content of 2.7, 2.2 and 0.52 mg L^{-1} of oxamic acid remained in the solutions upon application of UVA-PEF, UVC-PEF and the combined UVA-/UVC-PEF, respectively. This corresponds to 3.1%, 2.5% and 0.06% of the initial TOC, being much lower than the TOC determined in the final solutions (see Table 1). This means that such solutions contained small amounts of other undetected products that were hardly destroyed by ˙OH and UVA or UVC light.

To better understand the photosensitivity of the Fe(III) complexes, a last series of assays was made. The Fe^{2+} regeneration in solutions containing 0.20 mM Fe^{3+} and 0.80 mM of each acid was determined upon irradiation with UVA or UVC light. Fig. S4 reveals a poor and steady photoreduction of $[Fe(OH)]^{2+}$ species from Reaction (3) and Fe(III)-oxamate complexes from Reaction (4), showing a higher Fe^{2+} regeneration using UVC instead of UVA photons In contrast, UVC became more effective during the first 60 min for the photolysis of Fe(III)-oxalate species and the first 30 min for the Fe(III)-tartrate ones,

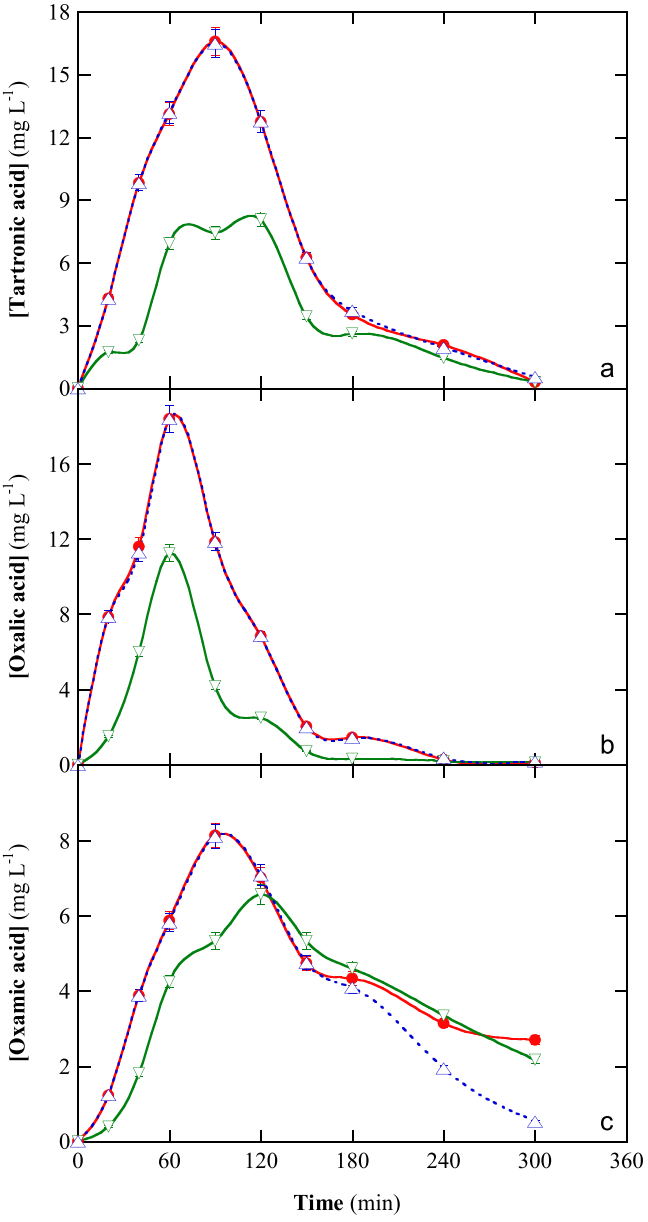

Fig. 7. Time course of the concentration of (a) tartronic, (b) oxalic and (c) oxamic acids detected during the mineralization of 200 mL of 20 mg L^{-1} BTH + 20 mg L^{-1} 2-OH-BTH in 0.050 M Na_2SO_4 with 0.20 mM Fe^{2+}, at pH 3.0 and 25 °C, by PEF using an IrO_2-based/GDE cell at 33.3 mA cm^{-2}. Lamp: (●) 6-W UVA, (▼) 8-W UVC and (■) 6-W UVA/8-W UVC (last 150 min).

whereupon a similar and quasi-steady state was reached with both lamps. These results suggest a slightly greater ability of UVC to photolyze such species, which becomes an additional explanation to justify the positive outcome of part-time use of UVC in UVA-PEF. It is also remarkable from Fig. S4 that the photosensitivity decreases in the order Fe(III)-oxalate > Fe(III)-tartronate > > Fe(III)-oxamate ≥ $Fe(OH)^{2+}$. This agrees with the quick and total removal depicted in Fig. 7a and b for the two former species, as well with the slower decay of Fe(III)-oxamate complexes shown in Fig. 7c.

4. Conclusions

This work has demonstrated that the upgrading of classical UVA-PEF process was feasible upon part-time use of UVC light, which allowed a higher mineralization at the expense of a relatively low increase of energy consumption (2 kW h (g TOC)$^{-1}$ under the best

conditions). UVC light was then slightly more efficient than UVA light to degrade BTH and 2-OH-BTH. The positive contribution of UVC photons can be mainly accounted for by the additional $^{\cdot}OH$ formation from photolytic homolysis of H_2O_2, which added to $^{\cdot}OH$ generated from Fenton's reaction. In addition, UVC light favored the direct photodegradation of the aromatic structures, as well as the photoreduction of Fe(III)-carboxylate complexes. Fe(III)-oxalate and Fe(III)-tartronate were particularly photosensitive, which promoted their overall mineralization in concomitance with Fe^{2+} regeneration. The disappearance of both BTs always agreed with a pseudo-first-order kinetics. SO_4^{2-} and NH_4^+ ions were released during the electrolyses. Five heteroaromatics were detected upon degradation of 2-OH-BTH. This compound was found as a by-product during BTH oxidation, which allows justifying the faster removal of the latter pollutant.

Declaration of Competing Interest

The authors declare that they have no known competing financial interests or personal relationships that could have appeared to influence the work reported in this paper.

Acknowledgements

The authors thank the financial support from project CTQ2016-78616-R (AEI/FEDER, EU) and PhD scholarship awarded to A. Xu (State Scholarship Fund, CSC, China).

Appendix A. Supplementary data

Supplementary material related to this article can be found, in the online version, at doi:https://doi.org/10.1016/j.apcatb.2019.118127.

References

[1] R. Ciriminna, L. Albanese, F. Meneguzzo, M. Pagliaro, ChemSusChem 9 (2016) 3374–3381.
[2] A. Ashgar, A.A.A. Raman, W.M.A.W. Daud, J. Clean. Prod. 87 (2015) 826–838.
[3] I. Sirés, E. Brillas, M.A. Oturan, M.A. Rodrigo, M. Panizza, Environ. Sci. Pollut. Res. 21 (2014) 8336–8367.
[4] P.V. Nidheesh, M. Zhou, M.A. Oturan, Chemosphere 197 (2018) 210–227.
[5] C.A. Martínez-Huitle, M.A. Rodrigo, I. Sirés, O. Scialdone, Chem. Rev. 115 (2015) 13362–13407.
[6] S. Lanzalaco, I. Sirés, M.A. Sabatino, C. Dispenza, O. Scialdone, A. Galia, Electrochim. Acta 246 (2017) 812–822.
[7] A. Xu, K. Wei, Y. Zhang, W. Han, J. Li, X. Sun, J. Shen, L. Wang, Electrochim. Acta 246 (2017) 1200–1209.
[8] A. Khataee, A. Khataee, M. Fathinia, B. Vahid, S.W. Joo, J. Ind. Eng. Chem. 19 (2013) 1890–1894.
[9] A. Khataee, A. Akbarpour, B. Vahid, J. Taiwan Inst. Chem. Eng. 45 (2014) 930–936.
[10] G. Coria, T. Pérez, I. Sirés, J.L. Nava, J. Electroanal. Chem. 757 (2015) 225–229.
[11] M. Panizza, M.A. Oturan, Electrochim. Acta 56 (2011) 7084–7087.
[12] M.S. Yahya, N. Oturan, K. El Kacemi, M. El Karbane, C.T. Aravindakumar, M.A. Oturan, Chemosphere 117 (2014) 447–454.
[13] O. Ganzenko, N. Oturan, I. Sirés, D. Huguenot, E.D. van Hullebusch, G. Esposito, M.A. Oturan, Environ. Chem. Lett. 16 (2018) 281–286.
[14] Z. Ye, E. Brillas, F. Centellas, P.L. Cabot, I. Sirés, Appl. Catal. B: Environ. 257 (2019) 117907.
[15] A. Thiam, I. Sirés, F. Centellas, P.L. Cabot, E. Brillas, Chemosphere 136 (2015) 1–8.
[16] A. Bedolla-Guzmán, I. Sirés, A. Thiam, J.M. Peralta-Hernández, S. Gutiérrez-Granados, E. Brillas, Electrochim. Acta 206 (2016) 307–316.
[17] R. Hernández, I. Olvera-Rodríguez, C. Guzmán, A. Medel, L. Escobar-Alarcón, E. Brillas, I. Sirés, K. Esquivel, Electrochem. Commun. 96 (2018) 42–46.
[18] E. Brillas, J. Braz. Chem. Soc. 25 (2014) 393–417.
[19] L.C. Almeida, S. Garcia-Segura, C. Arias, N. Bocchi, E. Brillas, Chemosphere 89 (2012) 751–758.
[20] E. Bocos, E. Brillas, M.A. Sanromán, I. Sirés, Environ. Sci. Technol. 50 (2016) 7679–7686.
[21] A. Thiam, E. Brillas, J.A. Garrido, R.M. Rodríguez, I. Sirés, Appl. Catal. B: Environ. 180 (2016) 227–236.
[22] S. Alcocer, A. Picos, A.R. Uribe, T. Pérez, J.M. Peralta-Hernández, Chemosphere 205 (2018) 682–689.
[23] Z. Ye, J.R. Steter, F. Centellas, P.L. Cabot, E. Brillas, I. Sirés, J. Clean. Prod. 208 (2019) 1393–1402.
[24] Z. Ye, D.R.V. Guelfi, G. Álvarez, F. Alcaide, E. Brillas, I. Sirés, Appl. Catal. B: Environ. 247 (2019) 191–199.
[25] F. Kaplan, A. Hesenov, B. Gözmen, O. Erbatur, Environ. Technol. 32 (2011) 685–692.
[26] F.C. Moreira, J. Soler, M.F. Alpendurada, R.A.R. Boaventura, E. Brillas, V.J.P. Vilar, Water Res. 105 (2016) 251–263.
[27] F.C. Moreira, J. Soler, A. Fonseca, I. Saraiva, R.A.R. Boaventura, E. Brillas, V.J.P. Vilar, Appl. Catal. B: Environ. 182 (2016) 161–171.
[28] A. Wang, Y. Zhang, H. Zhong, Y. Chen, X. Tian, D. Li, J. Li, J. Hazard. Mater. 342 (2018) 364–374.
[29] C. Espinoza, J. Romero, L. Villegas, L. Cornejo-Ponce, R. Salazar, J. Hazard. Mater. 319 (2016) 24–33.
[30] Y. Zhang, A. Wang, X. Tian, Z. Wen, H. Lv, D. Li, J. Li, J. Hazard. Mater. 318 (2016) 319–328.
[31] T. Pérez, I. Sirés, E. Brillas, J.L. Nava, Electrochim. Acta 228 (2017) 45–56.
[32] J.R. Steter, E. Brillas, I. Sirés, Appl. Catal. B: Environ. 224 (2018) 410–418.
[33] I. Salmerón, K. Plakas, I. Sirés, I. Oller, M.I. Maldonado, A.J. Karabelas, S. Malato, Appl. Catal. B: Environ. 242 (2019) 327–336.
[34] M. Panizza, G. Cerisola, Chem. Rev. 109 (2009) 6541–6569.
[35] R.S. Keri, M.R. Patil, S.A. Patil, S. Budagumpi, Europ. J. Med. Chem. 89 (2015) 207–251.
[36] W. Liu, J. Xue, K. Kannan, Sci. Total Environ. 592 (2017) 91–96.
[37] A. Maceira, R.M. Marcé, F. Borrull, Chemosphere 193 (2018) 557–566.
[38] F. Zeng, J.P. Sherry, N.C. Bols, Chemosphere 155 (2016) 308–318.
[39] A.G. Asimakopoulos, A. Ajibola, K. Kannan, N.S. Thomaidis, Sci. Total Environ. 452–453 (2013) 163–171.
[40] R. Karthikraj, K. Kannan, Chemosphere 181 (2017) 216–223.
[41] A. Kloepfer, M. Jekel, T. Reemtsma, Environ. Sci. Technol. 39 (2005) 3792–3798.
[42] L. Wang, J. Zhang, H. Sun, Q. Zhou, Environ. Sci. Technol. 50 (2016) 2709–2717.
[43] A.G. Asimakopoulos, A.A. Bletsou, Q. Wu, N.S. Thomaidis, K. Kannan, Anal. Chem. 85 (2013) 441–448.
[44] N. Haroune, B. Combourieu, P. Besse, M. Sancelme, T. Reemtsma, A. Kloepfer, A. Diab, J.S. Knapp, S. Baumberg, A.-M. Delort, Appl. Environ. Microbiol. 68 (2002) 6114–6120.
[45] A.A. Mazioti, A.S. Stasinakis, G. Gatidou, N.S. Thomaidis, H.R. Andersen, Chemosphere 131 (2015) 117–123.
[46] Y. Li, Q. Hu, C.-H. Chen, X.-L. Wang, D.-W. Gao, Bioresour. Technol. 236 (2017) 1–10.
[47] S. Bahnmüller, C.H. Loi, K.L. Linge, U. von Gunten, S. Canonica, Water Res. 74 (2015) 143–154.
[48] E. Borowska, E. Felis, J. Kalka, Chem. Eng. J. 304 (2016) 852–863.
[49] H. Valdés, C.A. Zaror, M. Jekel, J. Adv. Oxid. Technol. 19 (2016) 338–346.
[50] R. Andreozzi, A. D'Apuzzo, R. Marotta, J. Hazard. Mater. B80 (2000) 241–257.
[51] M.-C. Nika, A.A. Bletsou, E. Koumaki, C. Noutsopoulos, D. Mamais, A.S. Stasinakis, N.S. Thomaidis, J. Hazard. Mater. 323 (2017) 400–413.
[52] T. Zhang, Y. Chen, T. Leiknes, Environ. Sci. Technol. 50 (2016) 5864–5873.
[53] M. Panizza, A. Dirany, I. Sirés, M. Haidar, N. Oturan, M.A. Oturan, J. Appl. Electrochem. 44 (2014) 1327–1335.
[54] A. Galia, S. Lanzalaco, M.A. Sabatino, C. Dispenza, O. Scialdone, I. Sirés, Electrochem. Commun. 62 (2016) 64–68.
[55] H.J. Kuhn, S.E. Braslavsky, R. Schmidt, Pure Appl. Chem. 76 (2004) 2105–2146.
[56] J.C. Murillo-Sierra, I. Sirés, E. Brillas, E.J. Ruiz-Ruiz, A. Hernández-Ramírez, Chemosphere 192 (2018) 225–233.
[57] F.J. Welcher, 6th ed., Standard Methods of Chemical Analysis vol. 2, R.E. Krieger Publishing Co Huntington, New York, 1975 part B.
[58] C. Tai, J.-F. Peng, J.-F. Liu, G.-B. Jiang, H. Zou, Anal. Chim. Acta 527 (2004) 73–80.
[59] J.R. Steter, E. Brillas, I. Sirés, Electrochim. Acta 222 (2016) 1464–1474.